Int J Adv Manuf Technol (2014) 73:23–33
DOI 10.1007/s00170-014-5811-x

ORIGINAL ARTICLE

Detection of micro gap weld using magneto-optical imaging during laser welding

Xiangdong Gao · Yuquan Chen

Received: 25 November 2013 / Accepted: 24 March 2014 / Published online: 4 April 2014

Abstract Accurate seam tracking plays a critical role in acquisition of good weld. During laser butt joint welding, the laser beam focus must be controlled to follow the weld trajectory. The key problem to be solved is the automatic identification of weld position. An approach to detect the micro gap weld (gap width is less than 0.05 mm) based on magneto-optical imaging (MOI) is proposed. The laser butt joint welding of carbon steel was carried out. A magnetic excitation device was used to magnetize the weldment, and it was found that magnetic field distribution at the weld was different from other regions. The magnetized weldment was detected by using a magneto-optical sensor, and magneto-optical images of the weld were captured. By analyzing and processing weld MO images with low contrast and strong magnetic field noises, the weld center position could be detected accurately. Weld MO images at different laser welding speeds were investigated to analyze the varieties of image characteristics. Experimental results indicated that the magneto-optical imaging technique could be applied to detect the micro gap weld accurately, which provides a novel approach for automatic identification and tracking of micro gap weld during laser welding.

Keywords Micro gap weld · Magneto-optical imaging · Laser welding · Seam tracking

1 Introduction

Laser welding has been widely used for its advantage in narrowly focusing laser radiation to a small area and high-intensity heat source, which is instrumental in realizing deep penetration and high-speed welding and improved mechanical properties [1–3]. However, this narrow area of laser weld fusion zone brings about problems of joint alignment and fit up. Small focus wandering off seam will result in lack of penetration or unacceptable weld. The weld position is determined by many parameters in the thermodynamic and physicochemical processes, such as weldment thermal deformation and laser welding speeds and so on [4, 5]. If an electromechanical or purely mechanical system is used to drive the weldment, many nonlinear factors will be inevitably introduced to the welding process and influence the system performance [6, 7]. The ability of detecting weld position is of primary concern in a laser welding process. Therefore, an auxiliary sensor should be used to detect and track the weld in real time.

The most popular technique used for weld detection and seam tracking is based on the principle of optical triangulation. A structured light is the process of projecting a known pattern of pixels (often grids or horizontal bars) on the weldment surface in front of laser beam focus, and the reflected scattered light is imaged back to a camera. The way allows vision systems to calculate the weld center information. The controller extracts information from the image and uses it for seam tracking. However, to detect the weld is a formidable task in that spatters and light disturbance are very strong during laser welding [8]. With regard to a laser butt joint welding where the weld gap is less than 0.05 mm, the reflected light deforms very small; the weld is too narrow to measure by using the principle of optical triangulation [9–11]. Using an ordinary camera to capture the micro gap weld whose width is less than 0.05 mm, the image gray value of weld during laser welding with much light radiation and spatters changes so small that it is difficult to identify the position of micro gap weld. Microscope can observe micro gap weld in a stationary state, but the depth of field of microscope is too small. During

X. Gao (✉) · Y. Chen
School of Electromechanical Engineering, Guangdong University of Technology, Guangzhou 510006, China
e-mail: gaoxd666@126.com

dynamic welding process, weldment moves by servo motor driving. The distance between weldment surface and microscope lens will fluctuate due to weldment heat distortion and welding mechanism vibration, and focal length will be changed. Therefore, the weld image will become blurry; the weld position cannot be detected easily. At present, there is no other effective automatic detecting and tracking methods for a micro gap butt joint welding.

Magneto-optical imaging (MOI) technology has been developed for inspection of cracks in aging aircrafts. This relatively new nondestructive test method gives an inspector the ability to quickly generate real-time images in aviation material surface and subsurface fine cracks. It is based on the combination of electromagnetic effect (eddy current or magnetic flux leakage) and the Faraday rotation effect. This technique became popular in the recent decade. Extensive research on MOI systems has been conducted in both imaging physics and image processing aspects at several groups. The main advantage of MOI is its fast and easy inspection capabilities in comparison to other conventional nondestructive inspection instruments. MOI inspection is up to 10 times faster than conventional eddy current methods because of its large inspection area and the ease of inspection and interpretation [12, 13]. Finite element analysis could be applied to aircraft rivet site inspection [14]. It was used to study parametric effects of threshold, frequency, and crack size on binary image production. There were many noises in MO images captured by a charge-coupled device (CCD) and a processor for real-time image. This led to the need for an image processing algorithm for reducing these background noises. MO images could be processed by motion-based filtering technique [15]. Image processing and automated classification algorithms were proposed for MO image analysis [16, 17]. These studies are mainly focused on crack inspection of aircraft rivets and other materials. In this paper, we study a new method to detect the position of micro gap weld in laser welding process using magneto-optical technique. The MOI characteristics of micro gap weld and detection method are different from those in literatures.

For laser micro gap butt joint welding, using MOI technology to detect weld is a new method. According to magnetic induction principle and Faraday rotation effect, it is necessary

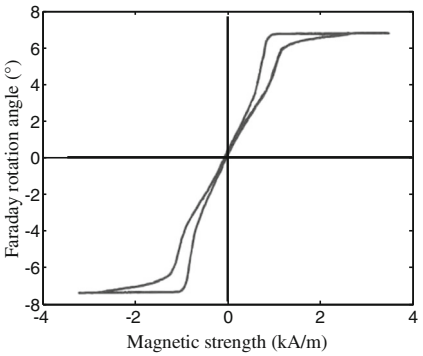

Fig. 2 Response curve between Faraday rotation angle and magnetic strength

to configure a MOI sensor and a magnetic excitation device to detect the weld during laser welding. Magnetic excitation device was used to magnetize the weldment, and it was found that magnetic field distribution at weld is different from other regions. The magnetized weldment was detected by using a MO sensor, and the MO images of weld were captured. By analyzing weld MO image features and characteristics, the weld position can be obtained, and the offset between laser beam focus and weld center can be measured in real time. Usually, there are much interferences such as spatter, plasma, and other radiation to influence on weld detection during laser welding. Unlike other visual sensing methods, the MOI method to detect weld is based on the induced magnetic field distribution on weldment surface. Using the MOI can avoid above interference and is expected to become an effective method for detecting micro gap weld.

The MOI equipment parameters that include operating frequency, source feeding current, and sensor parameters need to be examined for each inspection configuration. It is extremely difficult to adjust these parameters without using a proper computational model of the configuration under tests [18]. This paper mainly focuses on a method to detect the offset between laser beam focus and weld position during laser welding, in which the weld width is less than 0.05 mm. The working principle of MOI device for detecting the weld is introduced, and the relationship between weld magnetic field and MO grayscale image is analyzed. In the process of detecting micro gap weld, the magnetic field is usually weak, and the signal related to weld is difficult to obtain in an

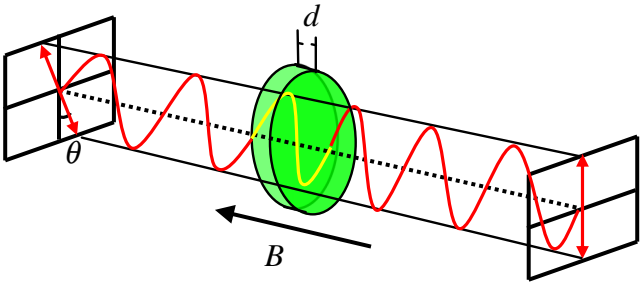

Fig. 1 Illustration of Faraday rotation effect

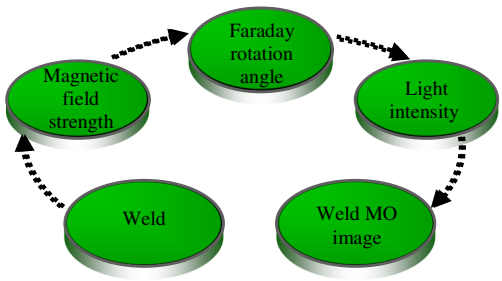

Fig. 3 Diagram of weld MOI principle

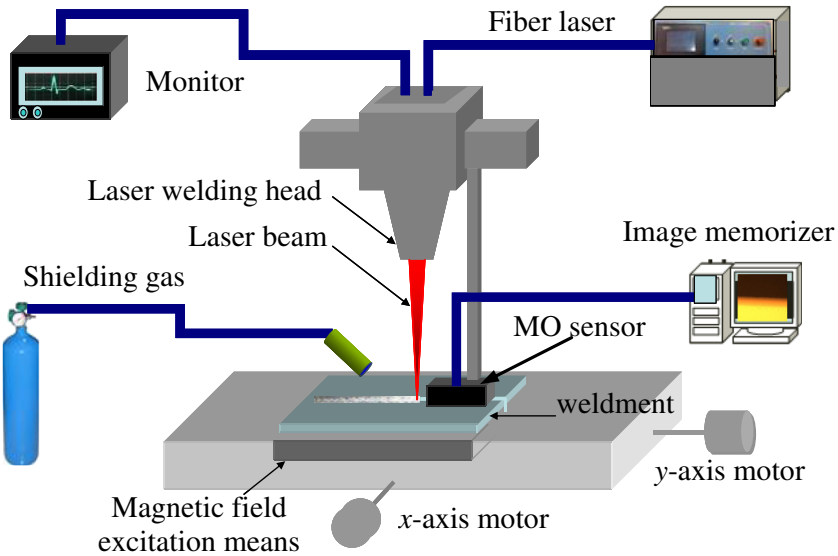

Fig. 4 Experimental setup of weld MOI and weld detection

environment of magnetic domains and other noises. It is important to eliminate the noises in order to enhance weld MO images; therefore, under low contrast and strong noise conditions, the image processing techniques are applied for weld MO images and calculating the weld position. The laser welding experiments were carried out at different welding speeds, and experimental results show that the MOI technology is effective to detect the micro gap weld.

2 MOI working principle

2.1 Faraday rotation effect

Faraday rotation effect is a magneto-optical phenomenon or an interaction between light and magnetic field. The rotation of polarization plane is proportional to the intensity of component of magnetic field in direction of light beam. When linearly polarized light passes through a glass in a direction that is parallel to the applied magnetic field, the plane of vibration will rotate (shown in Fig. 1). The relation between angle of polarization rotation and magnetic field observed for any given substance is found experimentally to be proportional to the magnetic induction strength (B) and to the distance (d) that light travels through the medium. This rotation can be expressed by the relation as follows:

$$\theta = VBd \tag{1}$$

where θ is the angle of rotation (in radians), B is the magnetic flux density in the direction of propagation (in teslas), d is the length (in meters) where light and magnetic field interact, and V is the Verdet constant for material. This empirical proportionality constant (in units of radians per tesla per meter) varies with wavelength and temperature and is tabulated for various materials [19].

For most MO media, the Faraday rotation angle is proportional to magnetic field strength. When a magnetic field exceeds a certain limit, the magnetization tends to saturation value; Faraday rotation angle also will tend to saturation at same time, shown in Fig. 2.

2.2 Weld MOI principle

When an electromagnet is placed upon or under a weldment, the excitation magnetic field on weldment surface is generated. The induced magnetic field at the weld will change when the weldment is excited by a magnetic field, and the vertical component of magnetic field at the weld is different from other region of weldment. When the optical film material and thickness are given, the degree of Faraday rotation angle is only related to the corresponding magnetic field strength [20]. The MO films convert magnetic field change into a corresponding change of light intensity. The intensity of linearly polarized light consists of the information of weld which is captured by a CMOS camera and then forms a 2-D real-time visualization image (weld MO image), which can be analyzed and processed by a computer.

Table 1 Laser welding conditions

Laser power P (W)	Welding speed V (mm/s)	Shielding gas Q (L/min)	Weldment $L\times W\times D$ (mm^3)	Weld width W_d (mm)	Weldment material
300	3.0–6.0	6	80×74×1.8	0–0.05	carbon steel

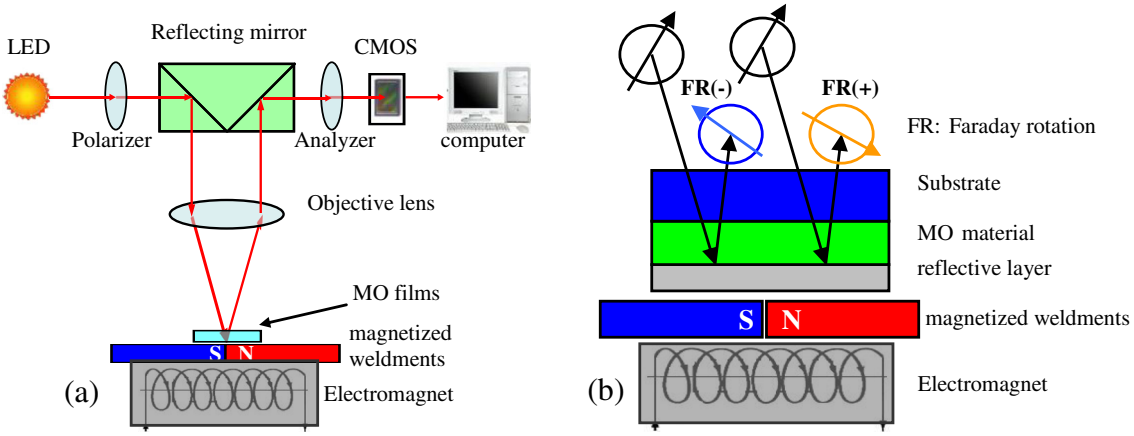

Fig. 5 Schematic diagram of magneto-optical sensor structure for weld detection. **a** Schematic diagram. **b** Weld MOI principle

According to Malus Law, if loss of light is neglected, the output light intensity (I) through the polarizer and analyzer can be expressed as follows:

$$I = I_0 \cos^2 \alpha \tag{2}$$

where I_0 is the input light intensity when transmission shaft angle between a polarizer and analyzer $\alpha=0$ or $\alpha=\pi$. When the magnetic induction strength is applied among two polarizes, considering Faraday rotation effect, the change of output light intensity can be expressed as follows:

$$I = I_0 \cos^2 (\alpha + \theta) \tag{3}$$

According to formula (3), given a certain α value, the output light intensity (I) has the relevant change when the angle (θ) changes. Faraday rotation angle (θ) is determined by the magnetic induction strength (B), and the weld leads to the magnetic field change. It can be seen that there exists a corresponding relation between the weld and MO images, as shown in Fig. 3, which shows the weld MOI basic principle.

3 MOI experimental setup

3.1 Laser welding device and welding conditions

Schematic drawing of experimental system is shown in Fig. 4. MOI experimental system consists of a YAG laser welding equipment (laser power 300 W); a MO sensor; a shielding gas (argon); and a welding experimental platform equipped with a camera, servomotors, and a fixing device. During a butt joint laser welding of carbon steel plate, in which the weld is less than 0.05 mm, the MO sensor is rigidly connected with the laser head. During laser welding, the laser head was stationary and the movement of weldment was controlled by a platform equipped with servomotors. The weldment was clamped over the platform which was within 2° of freedom in horizontal plane. The platform was driven by x-axis and y-axis servo motors. Theoretically, the closer the MO sensor with a molten pool, the higher the weld detection accuracy. However, there is much laser radiation to influence the weld detection accuracy when distance between MO sensor and a molten pool is closer. To avoid interference, the sensor must maintain a certain distance to a molten pool and laser head. Considering corresponding factors, this horizontal distance was adjusted to be about 55 mm between a MO sensor and a molten pool. Also, there was isolation between MO sensor and laser head. So, laser radiation had little effect on the weld MO images. Laser welding conditions are shown in Table 1.

3.2 MOI device and MO sensor parameters

Figure 5 shows the schematic drawing of weld MO detecting device, which shows the weld detecting process. The weld detecting device consisted of an optical system, MO films, a magnetic field excitation means, a light-emitting diode (LED) light source, and a complementary metal-oxide semiconductor (CMOS) sensor. The MO material was epitaxial grown bismuth-substituted rare-earth-iron-garnet with a thickness of 4 to 5 μm. For using a magneto-optical film as sensor in

Table 2 Parameters of MO sensor

Light	Wavelength λ (nm)	MO films $L \times W$ (mm^2)	Sensor resolution (pixel^2)	Pixel ratio size K (pixel/mm)	Magnetic field H (kA/m)	Sensor sampling rate F (f/s)
LED	590	20×15	2,592×1,944	102	[−2, 2]	25

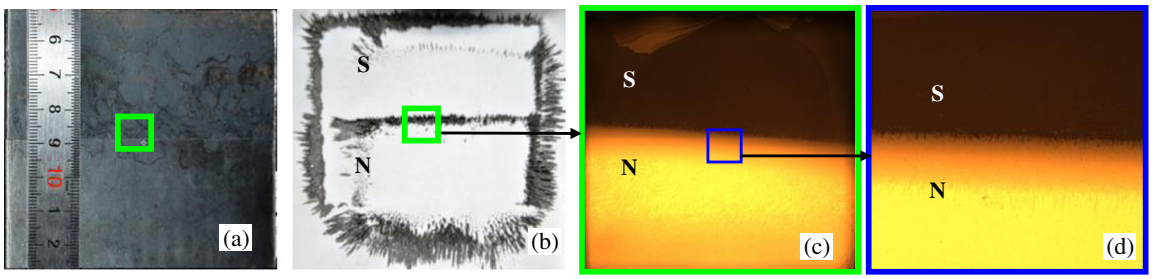

Fig. 6 Weldment photo, weld magnetic field distribution, and weld MO image. **a** Weldment. **b** Real magnetic field distribution of weld. **c** Weld MO image. **d** Local magnification MO image of weld

reflexion mode, the film is mirrored by a dielectric mirror. According to MOI system working principle, when a LED light passes through the polarizing plate, the linearly polarized incident light is obtained and focused on the magneto-optical film by the objective lens [21]. After reflected by reflection mirror, polarization light direction rotates and light signal is captured and imaged by a CMOS. Figure 5b shows the micro diagram of MO sensor for weld detection. The induced magnetic field to weldment surface which was magnetized by an electromagnet had a direct effect on MO films. The polarization plane of polarized light produced different degrees of rotation and led to the changes of light intensity. Table 2 shows the detailed parameters of MO sensor. Apparently, the closer the distance between MO sensor and weldment surface, the clearer the weld MO image. In order to prevent MO sensor damage from high temperature and spatter in laser welding process, the sensor should have a proper vertical distance to weldment surface. Considering the above factor effect, this distance was adjusted to be 2.5 mm during welding experiments.

A weldment photo, a magnetic field distribution of weld, and a weld MO image are shown in Fig. 6. To obtain the characteristics of the weld MO image, a definite area in the middle of the weldment containing the information of the weld magnetic field is observed in Fig. 6a. Figure 6b shows the real magnetic field distribution image of the weld. The magnetic field strength is largest at two edges of weld of magnetized weldment. The magnetic field distribution of weld can be imaged and detected by a MO sensor. In Fig. 6c, the information of weld can be observed clearly from MO image, and the detailed location of weld is shown in a local magnification image (Fig. 6d), where the magnetic field corresponding to two edge regions (N pole, S pole) reaches saturation. According to Fig. 2, Faraday rotation angle becomes saturated. In a MO image, S pole area is black and N pole area is bright. So, the two regions present obvious chromatic aberration. According to gray value distribution of the weld, we can easily judge the weld position in a MO image.

4 Analysis of experimental results

4.1 Obtaining weld MO images

The dynamic MO images were captured at different welding speeds. A total of four sets of data were collected, each set contained about 650 frames of MO images. Figure 7 shows a local magnification image sequence of weld captured by a MO sensor, in which image size is 624×656 pixel^2. The drastic changes of gray value in the MO image show that the weld regional characteristics are so obvious at the weld that the weld position can be clearly identified.

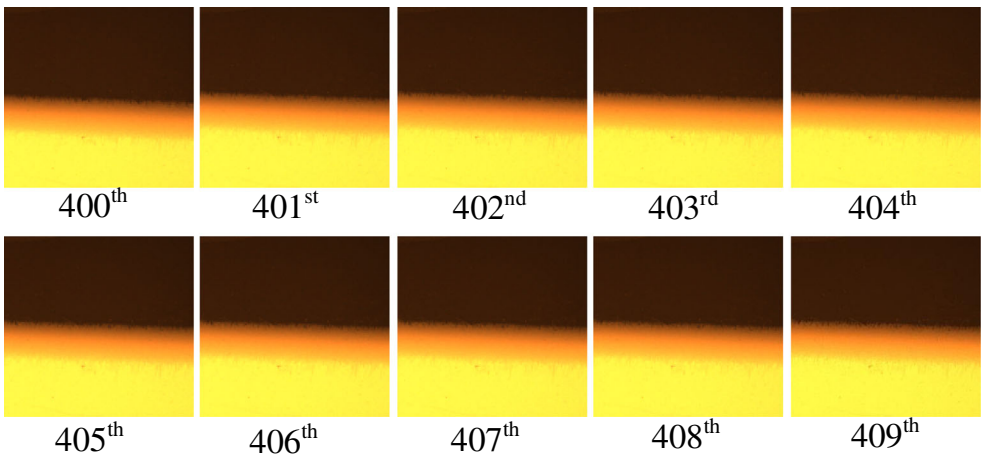

Fig. 7 Dynamic image sequences of weld captured by a MO sensor

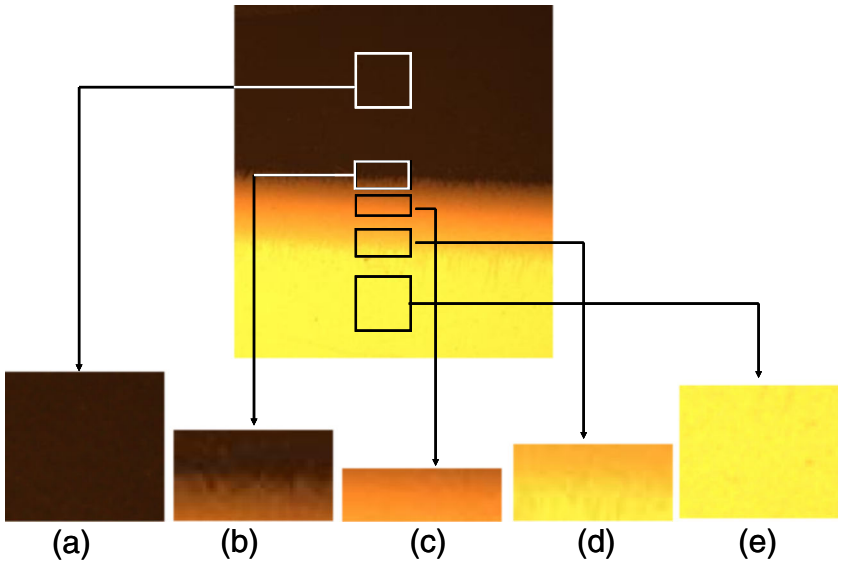

Fig. 8 Exploded view of the 400th MO image. **a** Upper part of weldment. **b** Upper edge of weld transition zone. **c** Weld center. **d** Lower edge of weld transition zone. **e** Lower part of weldment

4.2 Weld MO image processing

The weld MO image is affected by a variety of factors. Figure 8 shows the 400th MO image in an image sequence, and Fig. 8a–e shows the exploded view of the MO image. The upper and lower parts of the MO image are corresponding to Fig. 8a, e, respectively, in which exist some noises including light intensity change and magnetic domain change. The smoothness on the weldment surface was reflected as a background noise in a MO image. Especially there were many tiny protrusions and depressions at the weld edges, it is nonsmooth and led the induced magnetic field distribution to be abnormal, thus caused a lot of noises in the MO image. For example, the local magnification image has a large amount of burrs in Fig. 8b–d. To obtain the accurate weld position, the weld MO image features must be enhanced by image processing.

Since the MO image contains many noises, the information of weld is difficult to be directly extracted. To position the weld accurately, the characteristics of MO images are analyzed by image processing to eliminate these noises. Figure 9a shows a weld MO grayscale image, and its histogram shows obvious double peaks in Fig. 9b. By analyzing the gray distribution, gray value appears obvious stratification at two intervals, [0, 40], [220, 255], where interval [0, 40] is S magnetic pole saturation region which is the black area of MO image, and interval [220, 255] is N magnetic pole saturation region which is the bright area. The gray value of weld is of uniform distribution in the interval [40, 220]. To extract the weld position coordinates, one column was selected to analyze the gray change from a grayscale image. Figure 10 shows the gray distribution of the 115th column, which is still divided into three intervals, [0, 40], [40, 220], [220, 255]. Point A is the lower edge of the weld area which corresponds to gray value of 40, and point B is the upper edge which corresponds to gray value of 220. The weld influences the magnetic field distribution, which is expressed in a MO image. In the weld gap, the direction of magnetic lines of flux is horizontal from the N pole to S pole. The vertical component of magnetic field strength is zero at the weld center. The magnetic field strength increases smoothly from zero at the weld center to the saturation of two ends in the MO image and forms a clear transition zone in interval [40, 220], which is called as the weld transition zone. As shown in Fig. 10, the weld transition zone from point A to point B is not a real weld. The weld transition zone reflects the magnetic field distribution status at the weld, not to be the actual weld width. The actual weld is the dividing line at the weld transition zone in Fig. 10, and its width is approximately 5 pixels. The main goal

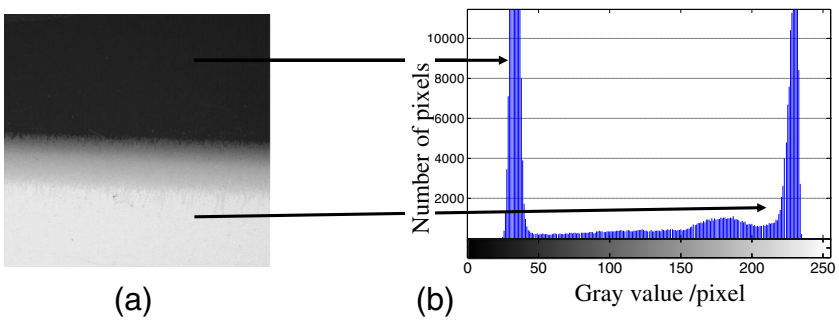

Fig. 9 Grayscale image and histogram of weld MO image. **a** Grayscale image. **b** Histogram

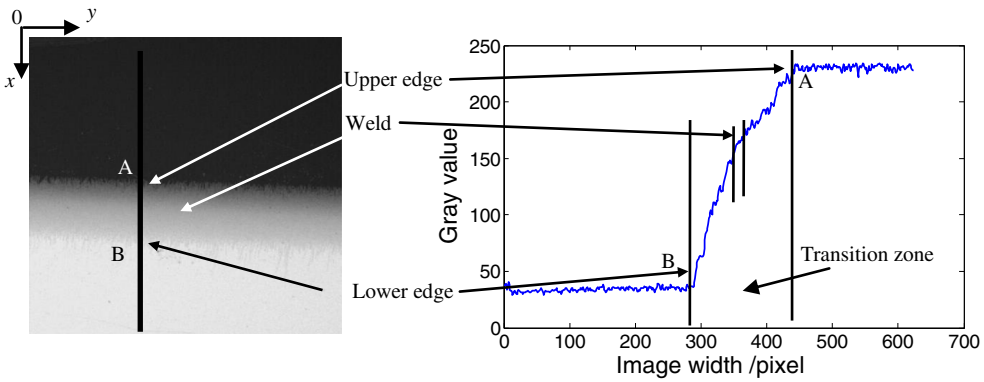

Fig. 10 Gray distribution of the 115th column in a weld MO image

of weld detection is that the weld position is accurately measured rather than the weld width. On the weldment surface, the induced magnetic field is symmetrical about the weld center. Therefore, the weld center position can be measured according to the weld transition zone width and the dividing line. The weld center is the midpoint of transition zone AB in Fig. 10, which can simply be given as follows:

$$x_C = (x_A + x_B)/2; y_C = (y_A + y_B)/2 \tag{4}$$

where (x_C, y_C) is the coordinate of the weld center, (x_A, y_A) is the coordinate of point A, (x_B, y_B) is the coordinate of point B, and y_C is also the selected column coordinate. Figure 11 shows a detailed flowchart of the weld MO image processing. By median filtering and using Canny edge detection, the weld center position coordinates are calculated easily. The weld center presents linear in a MO image and matches with the actual weld line. The MOI method according to magnetic field symmetry principle about the weld center on the weldment does not require an accurate measurement of weld width.

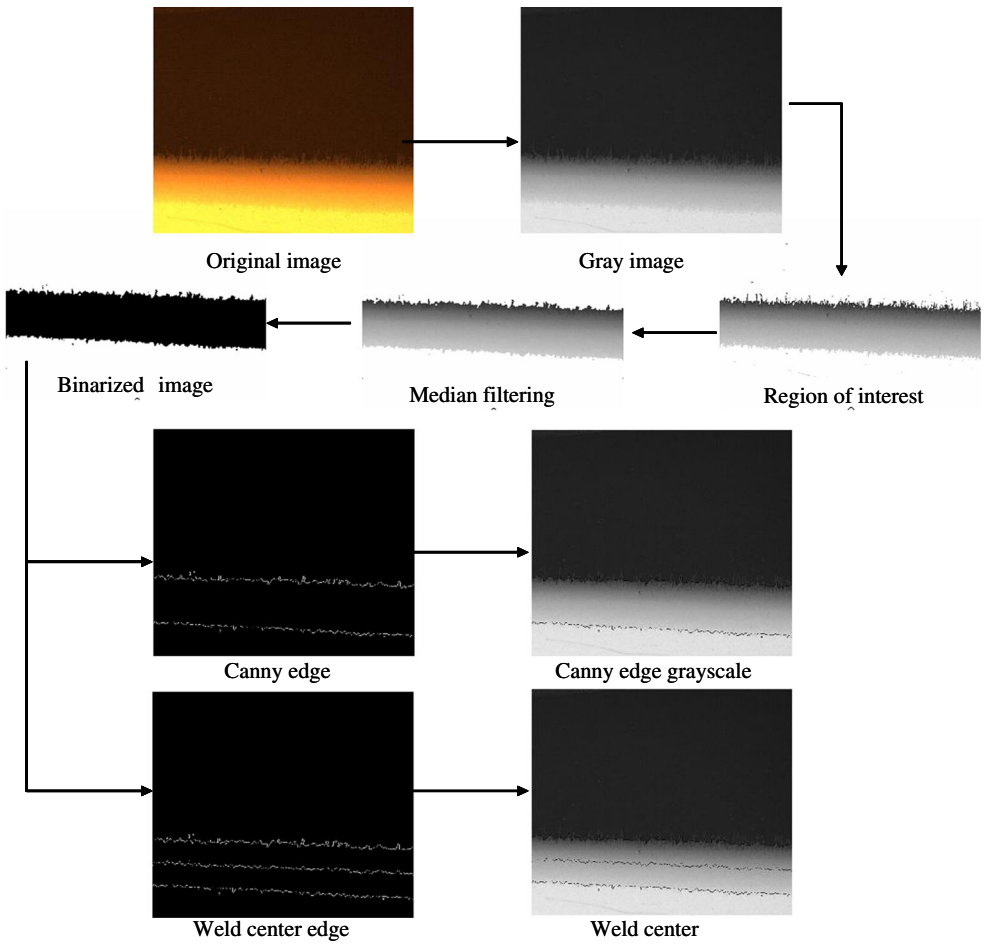

Fig. 11 Flowchart of weld MO image processing

According to the weld transition zone of symmetrical magnetic field, the weld center can be directly extracted. Compared with the traditional methods, the transition zone is equivalent to enlargement of the weld and contributes to acquisition of weld center.

4.3 Extraction of weld position parameter and calculation of weld offset

To verify the effectiveness of micro gap MOI method, the weld detection experiments are designed as follows, the welding trajectory was set to be an oblique line shown in Fig. 12a, and a MO sensor was upon the surface of weldment. At welding start point, the MO sensor detected the area on weld left and was gradually approaching the weld center line, then went across the joint to reach the end point on the weld right. The length of welding path is 77.5 mm. Meanwhile, to verify the accuracy of MOI method, Fig. 12b is captured by using the built-in camera of laser welding device whose magnification is 40 times. The cross center is the focus of MO sensor detecting location, and black line is the weld. The actual offset can be accurately measured between MO sensor and weld center in Fig. 12b. At the same time, the weld center position parameter could be extracted from each MO image by using the image processing algorithm. The measured offset between weld center and MO sensor focus can simply be given as follows:

$$E_i = (p_i - c), i = 1, 2, 3 \ldots n \tag{5}$$

where p_i is the weld center position parameter extracted from MO image, c is the position of MO sensor focus, E_i is the measured value of weld offset, and n is the number of image sequence. In laser welding process, laser head and sensor did not move; the weldment was controlled movement by a platform, so the value of c was fixed.

To obtain the characteristics of MO sensor wandering off the weld, a definite area in the middle of the MO image

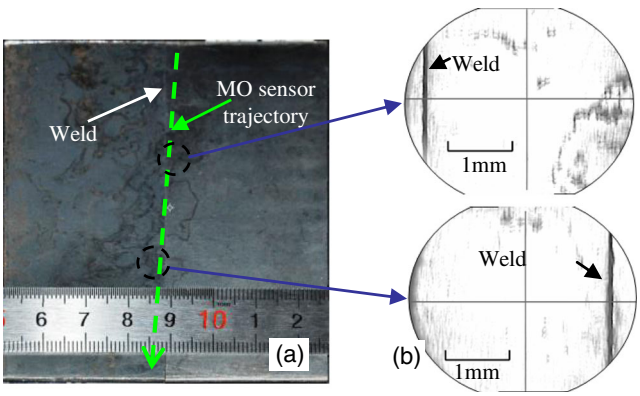

Fig. 12 Weld and MO sensor detection trajectory. **a** Schematic of MO sensor detection trajectory. **b** Offset between MO sensor and weld

containing the information of the weld position is observed. According to the MOI method, we can easily judge the weld center position. Under the welding speed of 3 mm/s condition, an image sequence containing 600 frames was captured by the MO sensor. The weld center position parameter could be extracted from each image by using the image processing algorithm in Fig. 11. For the whole image sequences, the detailed position of weld center can be shown in Fig. 13. The weld trajectory is nearly a straight line. At the region M shown in Fig. 13a, when the MO sensor started to capture the MO images, the laser welding did not start; the MO sensor position was fixed on the top of weldment. So, the measured offset of the weld center did not change and became a horizontal straight line. Similarly, at the region N, the laser welding had completed a predetermined distance to stop, but

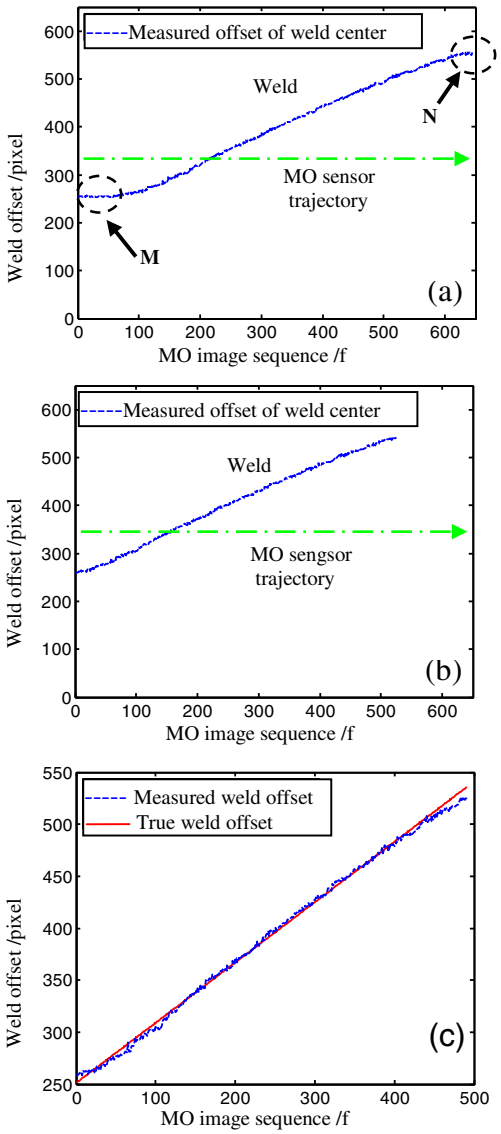

Fig. 13 True and measured weld offset. **a** Measured weld offset at the whole region. **b** Measured weld offset at the effective detecting region. **c** True and measured weld offset at the effective region

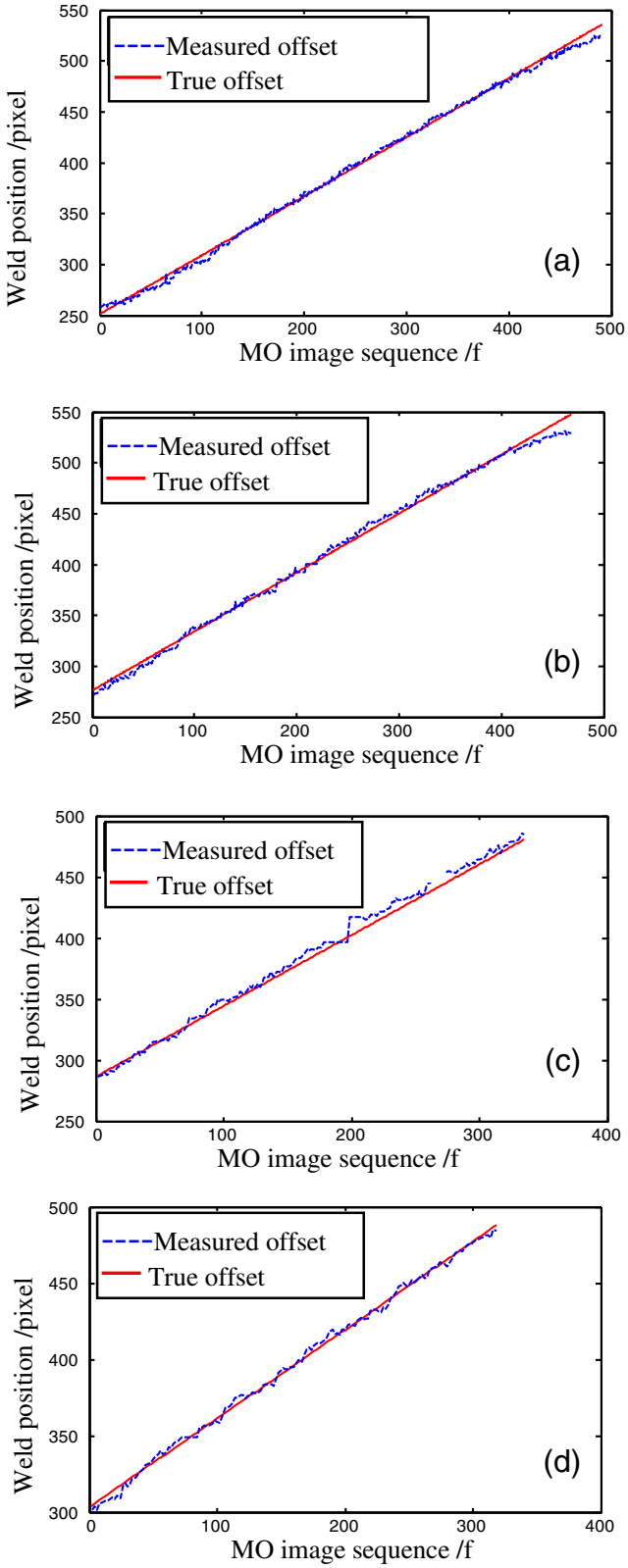

Fig. 14 True and measured values of weld offset. **a** Welding speed is 3 mm/s. **b** Welding speed is 4 mm/s. **c** Welding speed is 5 mm/s. **d** Welding speed is 6 mm/s

the MO sensor did not stop capturing the images; the measured offset trajectory was still close to a horizontal line. As shown in Fig. 13b, the invalid regions M and N can be removed in image processing and only leave the effective detection area of weld offset. To test the performance of MOI method, the results of true and measured weld offset are compared in Fig. 13c, where a true weld offset curve is obtained by using the built-in camera of laser welding device in Fig. 12b. The measured weld offset is close to the true weld offset, which means that the measured value of weld center position are approximately the true values of weld center.

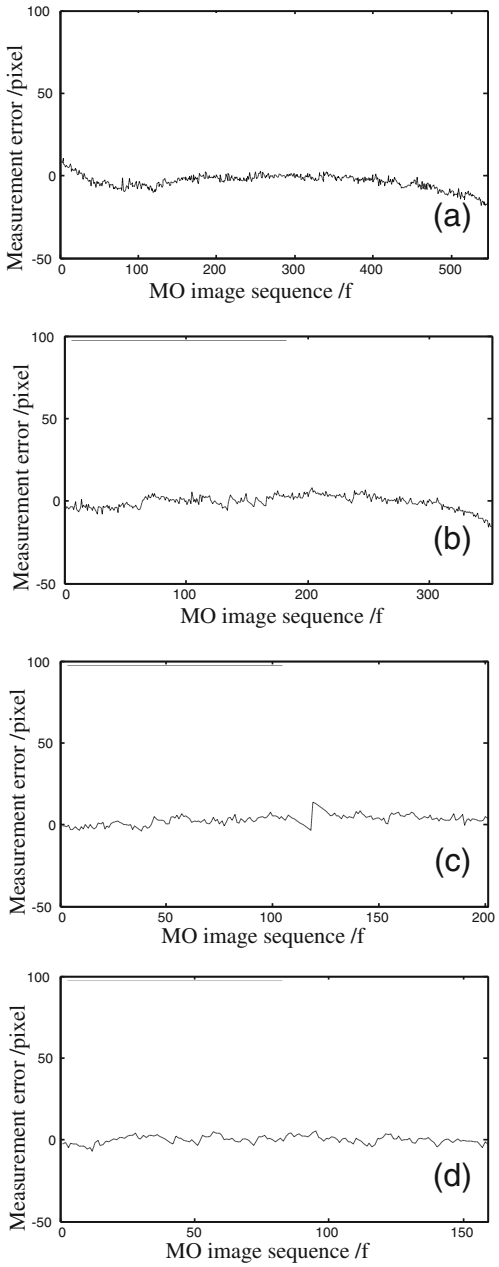

Fig. 15 Weld detection error curve. **a** Welding speed is 3 mm/s. **b** Welding speed is 4 mm/s. **c** Welding speed is 5 mm/s. **d** Welding speed is 6 mm/s

Table 3 Measurement error statistics of weld

	Error statistics e (mm)			
Welding speed (mm/s)	3	4	5	6
Sum of absolute error	10.9951	10.7373	7.0512	2.8036
Mean of absolute error	0.0242	0.0366	0.0344	0.0179
Variance $\times 10^{-4}$	2.8087	5.2456	5.3650	1.8623
Root variance	0.0168	0.0229	0.0232	0.0136
Maximum	0.0598	0.1032	0.1324	0.0527
Minimum	−0.0832	−0.0515	−0.0389	−0.0679

To verify the stability of MO sensor, many experiments have been conducted in which the welding speeds were 3, 4, 5, and 6 mm/s, respectively. The MO image recording speed was carried out at 25 f/s by the MO sensor. The comparisons of true offset and measured offset at effective detection region are shown in Fig. 14. Because the welding speed was different, the coordinate of absolute weld position in the MO image was also different at same sampling time. To simplify the comparison process of weld offset at four tests, the weld offset of effective detection region was given after standardization. As can be seen in Fig. 14, the measured values of weld offset are near the true values. The weld could be detected with satisfying accuracy.

4.4 Analysis of measurement errors

To evaluate the effectiveness of experimental results and MOI method, the error of weld detection is defined as follows:

$$e_i = y_i - n_i, i = 0, 1 \ldots n \tag{6}$$

where e_i is the error, γ_i is the weld position measured by MO sensor, and η_i is the true weld position. The weld detection errors are shown in Fig. 15, in which the error fluctuates around zero. It can be seen that the MOI method is effective and steady at different welding speeds. In addition, absolute error and root variance are introduced to estimate the stability of the weld detection. Mean value of absolute error, sum of absolute error, variance, root variance, maximum value, and minimum value at different welding speed experiments have been calculated, and the result is shown in Table 3. The mean value of absolute error is close to 0.03 mm, and the value of root variance is 0.02 under the different welding speed conditions. It means that the proposed method could have the high accuracy and stability of weld detection.

5 Conclusions

This paper has proposed a MOI method which uses a MO sensor to detect the micro weld position. In laser welding process, the MOI configuration is designed based on Faraday magneto-optical imaging technique that can be applied to convert magnetic field into MO image of weld. By image processing techniques, micro gap weld whose width is less than 0.05 mm can be identified in the MO image and the weld position can be accurately extracted and measured.

Based on this approach, the welding experiments were carried out. Though the measurement values of weld fluctuate around the actual position, the measurement error can meet with the detection accuracy in actual welding. Experimental results have demonstrated that the proposed methods are effective to detect the weld position from the MO images, which provide a novel approach for automatic identification and tracking of micro gap weld during laser welding.

Acknowledgments This project was supported by the National Natural Science Foundation of China (Grant no. 51175095) and the Natural Science Foundation of Guangdong Province, China (Grant no. 10251009001000001).

References

1. Gao XD, You DY, Katayama S (2012) Infrared image recognition for seam tracking monitoring during fiber laser welding. Mechatronics 22(4):370–380
2. Shao Y, Wang ZZ, Zhang YM (2011) Monitoring of liquid droplets in laser-enhanced GMAW. Int J Adv Manuf Technol 57:203–214
3. Riahi M, Amini A (2013) Effect of different combinations of tailor-welded blank coupled with change in weld location on mechanical properties by laser welding. Int J Adv Manuf Technol 67:1937–1945
4. Hamidinejad SM, Hasanniya MH, Salari N, Valizadeh E (2013) CO2 laser welding of interstitial free galvanized steel sheets used in tailor welded blanks. Int J Adv Manuf Technol 64(1–4):195–206
5. Gao X, Mo L, Wen Q, Katayama S (2013) Neural network model for recognizing joint offset during fiber laser welding. Weld J 92(9):251–257
6. Steele J, Mnich C, Debrunner C, Vincent T, Liu S (2005) Development of closed-loop control of robotic welding process. Int J Adv Manuf Technol 32(4):350–355
7. Gao XD, Wen Q (2013) Monitoring of High-power fiber laser welding based on principal component analysis of molten pool configuration. Laser Phys 23:126001–126008
8. Huang W, Kovacevic R (2012) Development of a real-time laser-based machine vision system to monitor and control welding processes. Int J Adv Manuf Technol 63(1–4):235–248
9. Quintino L, Costa A, Miranda R, Yapp D, Kong CJ (2007) Welding with high power fiber lasers—a preliminary study. Mater Des 28(4):1231–1237
10. Xu D, Fang Z, Chen H (2012) Compact visual control system for aligning and tracking narrow butt seams with CO2 gas-shielded arc welding. Int J Adv Manuf Technol 62:1157–1167

11. Gao XD, You DY, Katayama S (2012) seam tracking monitoring based on adaptive Kalman filter embedded Elman neural network during high power fiber laser welding. IEEE Trans Ind Electron 59(11):4315–4325
12. Fitzpatrick GL, Thome DK, Skaugset RL, Shih EY, Shih WC (1993) Magneto-optic/eddy current imaging of aging aircraft: a new NDI technique. Mater Eval 51(12):1402–1407
13. Fitzpatrick GL, Thome DK, Skaugset RL, Shih WC (1996) Magneto-optic/Eddy current imaging of subsurface corrosion and fatigue cracks in aging aircraft. Rev Prog Quant Nondestruct Eval 15: 1159–1166
14. Zeng Z, Liu X, Deng Y, Udpa L, Xuan L, Shih WC, Fitzpatrick GL (2006) A parametric study of magneto-optic imaging using finite-element analysis applied to aircraft rivet site inspection. IEEE Trans Magn 42(11):3737–3744
15. Park U, Udpa L, Stockman GC (2004) Motion-based filtering of magneto-optic imagers. Image Vision Comput 22(3):243–249
16. Udpa L, Shih WCL, Fitzpatrick GF (2001) Improved magneto-optic sensors for detection of subsurface cracks and corrosion in aging aircraft, in Proc. 5th Joint NASA/FAA/DoD Conf. Aging Aircraft, Orlando, FL, Sep 10–13
17. Deng Y, Zeng Z, Tamburrino A (2007) Automatic classification of magneto-optic image data for aircraft rivet inspection. Int J Appl Electromagn Mech 25:375–382
18. Cheng YH, Zhou ZF (2006) Application of the magneto-optic Faraday effect in NDT. INSIGHT 48(5):290–293
19. Radtke U, Zielke R, Rademacher HG, Crostack HA, Hergt R (2001) Application of magneto-optical method for real-time visualization of eddy currents with high spatial resolution for nondestructive testing. Opt Lasers Eng 36(3):251–268
20. Liu GQ, Le ZQ, Shen DF (2001) Magnetooptics. Shanghai Science and Technology Press, Shanghai, pp 43–45
21. Cheng Y, Jiang S, Luo G (2010) Visual detection of sub-surface defects using enhanced eddy current microscope. COMPEL 29(2):347–354